Low-temperature nonequilibrium transport in a Luttinger liquid

Ulrich Weiss[1], Reinhold Egger[2] and Maura Sassetti[3]
[1] *Institut für Theoretische Physik, Universität Stuttgart, D-70550 Stuttgart, Germany*
[2] *Fakultät für Physik, Albert-Ludwigs-Universität, D-79104 Freiburg, Germany*
[3] *Istituto di Fisica di Ingegneria, Università di Genova, I-16146 Genova, Italy*

arXiv:cond-mat/9509150v1 25 Sep 1995

The temperature-dependent nonlinear conductance for transport of a Luttinger liquid through a barrier is calculated in the nonperturbative regime for $g = 1/2 - \epsilon$, where g is the dimensionless interaction constant. To describe the low-energy behavior, we perform a leading-log summation of all diagrams contributing to the conductance which is valid for $|\epsilon| \ll 1$. With increasing external voltage, the asymptotic low-temperature behavior displays a turnover from the $T^{2/g-2}$ to a universal T^2 law.

PACS numbers: 72.10.-d, 73.40.Gk

I. INTRODUCTION

The interplay between electron-electron interactions and disorder has attracted a great deal of recent interest in condensed-matter theory. Many-body correlations play an essential role in quasi-one-dimensional (1D) fermionic systems, where the usual Fermi liquid behavior is destroyed by the interactions. The generic behavior of many interacting 1D fermion systems is instead described in terms of the Luttinger liquid model.[1,2] One may then ponder how transport in such a 1D "quantum wire" is affected by the presence of impurities or tunnel barriers. A quantitative answer to this question is of immediate interest for several experimental setups, e.g. the tunneling of edge state excitations in the fractional quantum Hall (FQH) regime,[3,4] or transport in narrow high-mobility heterostructure channels.[5,6]

The effect of one or a few barriers on the conductance of a Luttinger liquid has first been studied by Kane and Fisher (KF).[7] The Luttinger liquid model captures the low-energy properties of correlated electron transport if two conditions are met: one has short-ranged electron-electron interactions (i.e. the long-range $1/r$ tail of the Coulomb potential is screened by nearby gates), and electron-electron backscattering (BS) merely constitutes an irrelevant perturbation.[8] For the spinless case, BS is the exchange process of forward scattering, and therefore it is included readily by a redefinition of the interaction constant. All effects of the electron-electron interaction are then encompassed in a single dimensionless parameter g, which is approximately given by $g \approx (1+U/2E_{\rm F})^{-1/2}$. Here, U measures the interaction strength and $E_{\rm F}$ is the Fermi energy. We will consider the case of repulsive interactions, where one has $g < 1$. The noninteracting Fermi liquid case is recovered for $g = 1$. An ideal realization of this model is found in the tunneling of edge state excitations in the FQH regime. As shown by Wen,[3] these excitations are described by a (chiral) Luttinger liquid with $g = \nu$, where ν is the filling factor. Since ν is a topological quantity controlled by the bulk properties of the FQH bar, this provides an excellent experimental testing ground.[4] In addition, recent transport experiments in 1D quantum wires[6] have revealed Luttinger liquid behaviors directly for correlated electrons.

It has been demonstrated that the presence of an impurity potential term (the simplest realization of disorder) leads to a metal-isolator quantum phase transition at $T = 0$ when going from attractive to repulsive electron-electron interactions.[7] For $g < 1$, any (whatsoever weak) barrier will therefore result in zero linear conductance, $G = 0$. One is then concerned with the low-energy properties of the conductance, i.e. the behavior of $G(T, V)$ in the limit $T, eV/k_{\rm B} \ll T_{\rm K}$, where the Kondo temperature $T_{\rm K}$ sets the appropriate scale (see below). As indicated by the RG flow, this is a nonperturbative problem for weak barriers, and the past few years have shown considerable effort being devoted to this problem.[3,7,9–12]

By using a simple scaling argument, Kane and Fisher argued that the linear ($V \to 0$) conductance should behave as $T^{2/g-2}$ in the asymptotic low-temperature regime.[7] They obtained this law from matching the RG flow in the nonperturbative regime onto the large-barrier perturbative flow, thereby exploiting universality arguments. On the other hand, any finite voltage leads to a g-independent (universal) T^2 power law instead of the $T^{2/g-2}$ behavior. As one can never be sure about the validity of scaling arguments, we believe it is of use to have exact results for the *nonequilibrium finite-temperature* transport as provided here. We note that the exact solution for the case $g = 1/2$ has already been given within the bosonized description.[13] The linear conductance for $g = 1/2$ has also been calculated within an equivalent fermionic model by Kane and Fisher,[7] who extended an earlier zero-temperature approach by Guinea[14] to finite temperatures. Since the laws $T^{2/g-2}$ and T^2 coincide for $g = 1/2$, however, it is crucial to consider $g \neq 1/2$. In this paper, we start out from a dynamical approach and present a nonperturbative leading-log summation for $G(T, V)$ in the range $g = 1/2 - \epsilon$ with $|\epsilon| \ll 1$. We

systematically calculate the conductance in form of the series

$$G(T,V) = \sum_j a_j \epsilon^j \ln^j[\max(k_{\rm B}T, eV)] \; . \qquad (1.1)$$

Our study is related to recent work by Matveev, Yue and Glazman.[9] They have carried out a leading-log summation for weak electron-electron interactions. For the Luttinger liquid, this would correspond to the case $g = 1 - \epsilon$ with $|\epsilon| \ll 1$. Since the Kondo temperature vanishes with an essential singularity as g approaches 1 from below, it is desirable to have similar nonperturbative results for stronger electron-electron interactions. Their technique relies crucially on the assumption of weak interactions and can therefore not be employed directly in other regions of parameter space.

Basically parallel to our work, a powerful approach based on the thermodynamic Bethe ansatz has been put forward by Fendley, Ludwig and Saleur[11] who studied the linear conductance at $g = 1/3$. They mapped the original boson model of the Luttinger liquid onto a massless odd boson model which is integrable.[15] A basis of massless fermion-type quasiparticles can be derived, in which the S matrix for impurity scattering can be calculated exactly. The distribution function and the density of states of these quasiparticles are given in terms of integral equations with kernels determined by the completely elastic and factorizable scattering matrix of the bulk. Expressed in terms of these quantities, a Boltzmann-type rate expression for the conductance may then be derived. Switching to a suitable momentum integral representation, our solution for the current obtained from a dynamical approach can be transformed such that we can read off the S matrix for impurity scattering, the pseudoenergy and the density of states of the quasiparticles for $g = 1/2 - \epsilon$ and finite voltage. Therefore, our dynamical approach provides an independent check for results obtained by the thermodynamic Bethe ansatz, and furthermore gives a nontrivial prediction for the density of states.

The outline of this paper is as follows. In Sec. II, we present the model for our study and give the formal solution. The general diagrammatic expansion is explained in Sec. III, and the leading-log summation based on this diagrammatic expansion is discussed in great detail in Sec. IV. Results for the asymptotic low-energy behavior as well as a conjecture for the exact solution are presented in Sec. V, followed by concluding remarks in Sec. VI. Some technical details of the leading-log calculations are given in the Appendix.

II. GENERAL FORMALISM

To describe the problem of correlated electron transport, we employ the standard bosonization method.[1,2,7] The fermion field operator is expressed in terms of two bosonic fields $\phi(x)$ and $\theta(x)$,

$$\psi^\dagger(x) \sim \sum_{n \ {\rm odd}} \exp[in(\sqrt{\pi}\theta(x) + k_{\rm F}x) + i\sqrt{\pi}\phi(x)] \; ,$$

where the boson fields obey the commutation relation

$$[\phi(x), \theta(x')] = -(i/2)\,{\rm sgn}(x - x') \; .$$

Taking short-range electron-electron interactions and neglecting backscattering, this leads to the generic Luttinger liquid Hamiltonian (we put $\hbar = 1$)

$$H_0 = \frac{v}{2} \int dx \left[g(\partial_x \phi)^2 + g^{-1}(\partial_x \theta)^2 \right] \; , \qquad (2.1)$$

where g is the dimensionless interaction constant and v denotes the sound velocity. The Fermi velocity is then given by $v_{\rm F} = gv$. For the physical case of repulsive interactions, one has $g < 1$. Although this model is universal, actual computations, e.g. of correlation functions, necessitate introduction of a non-universal cutoff parameter $\omega_{\rm c}$ which is related to the bandwidth of the non-interacting problem. In the end, since H_0 is quadratic, everything can be solved exactly.[1]

To model the impurity, we follow KF[7] and consider a short-ranged scattering potential centered at $x = 0$. Omitting irrelevant multi-electron backscattering processes, the important contributions are captured by the $2k_{\rm F}$-component V_0 of this scattering potential, and one has

$$H = H_0 + V_0 \cos[2\sqrt{\pi}\theta(0)] + eV\,\theta(0)/\sqrt{\pi} \; . \qquad (2.2)$$

We have also included an external voltage V by assuming the voltage drop to occur at the barrier. This is well justified for not too small barriers.

The model (2.2) describes scattering by an impurity potential with effective strength V_0. Interestingly, results for a very high barrier $V_0 \gg \omega_{\rm c}$ can be obtained via an exact duality[16] from the case $V_0 \ll \omega_{\rm c}$. For $g < 1$, the large-barrier problem can be treated in lowest order in the number of tunneling transitions for any T and V, whereas in the weak-barrier case perturbation theory in V_0 is not possible at sufficiently low temperature and small voltage. Our subsequent treatment deals with the interesting nonperturbative regime. Putting $g = 1/2 - \epsilon$, our results presented in Sec. V hold under the conditions

$$V_0/\omega_{\rm c} \ll 1 \; , \quad |\epsilon| \ll 1 \; , \quad eV/k_{\rm B}T_{\rm K} \ll 1 \; , \quad T/T_{\rm K} \ll 1 \; , \qquad (2.3)$$

where $T_{\rm K}$ is the Kondo temperature

$$T_{\rm K} = (\sqrt{\pi}V_0/\omega_{\rm c})^{g/(1-g)}\sqrt{\pi}V_0/k_{\rm B} \qquad (2.4)$$

taken at $g = 1/2 - \epsilon$. The Kondo temperature provides an estimate for the extent of the nonperturbative regime.

Note that $T_{\rm K} \to 0$ for $g \to 1^-$ as alluded to in the Introduction.

In the following, we study the nonlinear static conductance $G(V,T) = \partial I/\partial V$. From the bosonized form of the current operator, it takes the form

$$G(V,T) = (e/\sqrt{\pi})\,(\partial/\partial V) \lim_{t\to\infty} \langle \dot\theta(0,t)\rangle \;, \qquad (2.5)$$

where $\langle \cdots \rangle$ denotes the thermal average over all modes of (2.2) away from $x = 0$. Remarkably, the model (2.2) is identical to the problem of a Brownian particle moving in a periodic potential.[13,14,16] This can be directly shown by a unitary transformation,[14] and we exploit such a mapping here. The θ-field taken at the location of the impurity, $\theta(0)$, corresponds to the position operator of the Brownian particle, and the Ohmic dissipation is provided by the plasmon modes away from the barrier. Thereby the conductance can be expressed in terms of the nonlinear mobility of the Brownian particle which is coupled to an Ohmic heat bath.

An exact formal expression for the conductance can be obtained from a real-time path-integral approach due to Feynman and Vernon.[17] Employing the unitary transformation of Eq. (2.2) onto the tight-binding limit of Brownian motion in a periodic potential, one can write this expression in a "Coulomb gas" representation of interacting discrete charges.[7] Alternatively, our expression (2.6) with (2.7) can be found by expanding the impurity propagator in terms of auxiliary charge paths.[16] The $\theta(0)$ paths can then be eliminated analytically and one has to sum over Hubbard-Stratonovich paths instead. These auxiliary paths can be parametrized by the discrete charges $\xi_j = \pm 1$.

In the end, the exact formal expression for the conductance takes the form of a power series in V_0^2,

$$G(V,T)/G_0 = 1 - (2\pi/eV)\,{\rm Im}\,U(V,T) \;, \qquad (2.6)$$

where $G_0 = ge^2/h$ and U describes the interacting charge gas

$$U(V,T) = \sum_{m=1}^{\infty} (iV_0)^{2m} \int_0^\infty d\tau_1\, d\tau_2 \cdots d\tau_{2m-1} \qquad (2.7)$$
$$\times \sum_{\{\xi\}} W_m \prod_{j=1}^{2m-1} e^{-igeV p_{j,m}\tau_j}\, \sin(\pi p_{j,m} g) \;,$$

with the interaction factor

$$W_m = \exp\left(\sum_{j>k=1}^{2m} \xi_j S(\tau_{jk}) \xi_k \right) \;. \qquad (2.8)$$

The interaction potential between the charges is given by

$$S(\tau) = 2g \ln[(\omega_{\rm c}/\pi k_{\rm B}T)\sinh(\pi k_{\rm B} T \tau)] \;. \qquad (2.9)$$

The $2m-1$ integration times τ_j in order V_0^{2m} are the intermediate times between the $2m$ successive charges, and τ_{jk} gives the time interval between charges ξ_j and ξ_k. Charge configurations $\{\xi\}$ contributing to (2.7) are restricted as follows. (1) In every order m, the $2m$ charges have zero total charge, $\sum_{j=1}^{2m} \xi_j = 0$ (neutrality condition). (2) The cumulative charge quantities $p_{j,m}$

$$p_{j,m} = \sum_{i=j+1}^{2m} \xi_i = -\sum_{i=1}^{j} \xi_i$$

can never be zero since otherwise the corresponding phase factor $\sin(\pi p_{j,m} g)$ would vanish. Expressed in graphical terms, there are no diagrams that can be subdivided into disjoint parts each of them representing a neutral configuration. (3) By convention, the first charge is $\xi_1 = -1$. With that, all $p_{j,m}$ are positive integers.

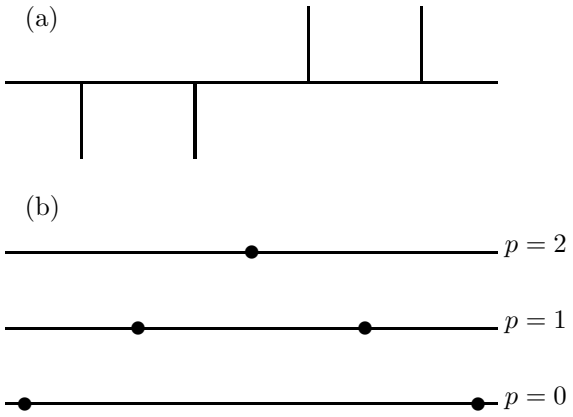


FIG. 1. Charge configuration $(--++)$ contributing in order $m = 2$ to the expression (2.7). (a) Diagram representing this configuration. Time flows along the horizontal line, vertical lines symbolize charges $\xi = \pm 1$. (b) Accumulated charge $p_i = \sum_{j>i} \xi_j$ during the course of the path. Circles stand for the momentary position of the path. For the shown configuration, an overall phase factor $2\pi\epsilon$ is acquired according to Eq. (2.10).

To illustrate these rules and our subsequent diagrammatic approach, Fig. 1 shows a charge configuration for $m = 2$ which does contribute to Eq. (2.7). Putting $g = 1/2 - \epsilon$, the phase factors appearing in Eq. (2.7) can be written as

$$\sin(\pi p g) \simeq \begin{cases} (-1)^{(p-1)/2} & , \quad p \text{ odd}, \\ \pi\epsilon p\,(-1)^{(p-2)/2} & , \quad p \text{ even}. \end{cases} \qquad (2.10)$$

As one moves away from $p = 0$, one has to pay the phase factors $1, 2\pi\epsilon, -1, -4\pi\epsilon, \ldots$ for dwelling on states labelled $p = 1, 2, 3, 4, \ldots$, respectively. This is displayed in Fig. 1(b). The charge configuration in Fig. 1 has a phase prefactor $2\pi\epsilon$. On the other hand, the breathing mode integral over the interior dipole [the τ_2-integration of the $(m = 2)$–term in Eq. (2.7)] has a $1/\epsilon$ singularity due to the $\tau^{-1+2\epsilon}$ short-time behavior of the intradipole interaction $\exp[-S(\tau)]$. Hence the combined expression is well defined even when $\epsilon = 0$.

The essential scale which separates the nonperturbative from the perturbative regime may be derived by using an adiabatic renormalization scheme.[18] Rather than working in frequency space, we take advantage of a time formulation. To obtain a renormalized frequency scale $\bar{\gamma}$, we integrate the length of a dipole from zero up to $1/\bar{\gamma}$, where the inverse time scale $\bar{\gamma}$ is self-consistently given by the short-time part of the breathing mode integral. We have

$$\bar{\gamma} = 2\pi\epsilon V_0^2 \int_0^{1/\bar{\gamma}} d\tau \, \frac{1}{(\omega_c \tau)^{1-2\epsilon}} = \frac{\pi V_0^2}{\omega_c} \left(\frac{\omega_c}{\bar{\gamma}}\right)^{2\epsilon} . \quad (2.11)$$

From this we obtain

$$\bar{\gamma} = \gamma \, (\omega_c/\gamma)^{2\epsilon} , \qquad \text{where} \quad \gamma = \pi V_0^2/\omega_c .$$

The frequency $\bar{\gamma}$ is the effective inverse time scale of the problem, and γ is the corresponding quantity when $\epsilon = 0$. The related temperature $\bar{\gamma}/k_B$ coincides with the previously introduced Kondo temperature (2.4) for $g = 1/2-\epsilon$.

To develop a general computational strategy, it is convenient to split up every time integral over the length of a dipole into a contribution from the short-time regime $0 < \tau < 1/\bar{\gamma}$ and a residual contribution from lengths $\tau > 1/\bar{\gamma}$. We shall refer to the short-time part as *collapsed dipole*. The crucial observation guiding us towards this terminology is as follows. Within leading-log accuracy, a collapsed dipole has zero dipole moment and therefore *no* interactions with other charges. This property allows us to carry out the grand canonical sum over all possible arrangements of collapsed dipoles between two confining charges in an exact manner. The strategy is then completed by developing a systematic scheme to calculate the contributions from all the residual time intervals $\tau_j > 1/\bar{\gamma}$ in the asymptotic low-energy regime (2.3).

There are two types of collapsed dipoles, namely $(+-)$ and $(-+)$. If they describe hops forth and back from states labelled by an *even* p value, the contributions of these two dipoles cancel each other completely. This is caused by the different sign of the phase factors $-\pi\epsilon p$ and $\pi\epsilon p$ which are connected with the dipoles $(-+)$ and $(+-)$, respectively. Hence there is no insertion of a gas of collapsed dipoles for the *even* time intervals $\tau_2, \tau_4, \ldots$ in Eq. (2.7), where the path is in an even p state. However, if the dipoles describe hops forth and back from states labelled by *odd* p, the dipoles $(-+)$ and $(+-)$ come with phase factors $\pi\epsilon(1+p)$ and $\pi\epsilon(1-p)$, respectively. Note that the second type does not contribute when $p = 1$. The sum of both contributions is independent of p. Allowing next that the collapsed dipole $(-+)$ [as well as $(+-)$] moves freely within an interval τ, we find a total contribution $-\bar{\gamma}\tau$. Finally, if we consider instead of the two dipoles a grand canonical noninteracting gas of these being confined within an odd-time interval τ, the total contribution is summed to an exponential factor $\exp(-\bar{\gamma}\tau)$.

To summarize these findings, the overall effect of the collapsed dipoles is to cause exponential suppression of every long odd time interval on a length $1/\bar{\gamma}$, while long even time intervals are *not* suppressed on this scale. In the diagrammatic expansion given below, we indicate the insertion of a grand canonical gas of collapsed dipoles by a square box. We shall refer to *bare* diagrams when they are free of collapsed dipoles and to *dressed* diagrams when every odd time interval is dressed by a square box.

III. DIAGRAMMATIC EXPANSION

In the following, we wish to evaluate the exact expression (2.6) with (2.7) for the nonlinear conductance in the low-energy regime specified in Eq. (2.3). In that case, a leading-log summation becomes possible around $g = 1/2$. With $g = 1/2 - \epsilon$, we compute the coefficients a_j in the series

$$G(V,T) = \sum_{j=0}^{\infty} a_j(V,T) \, \epsilon^j \ln^j[\max(k_B T, eV)] . \quad (3.1)$$

Contributions $\sim \epsilon^k \ln^j[\max(k_B T, eV)]$ with $j < k$ are disregarded in our calculation. This approximation is valid under conditions (2.3). In this section, computation of the functions $a_j(V,T)$ is presented in detail.

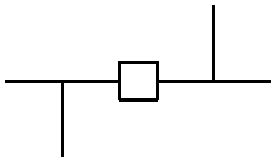


FIG. 2. Diagram giving the contribution U_1 to the conductance. The square stands for a factor $\exp[-\bar{\gamma}\tau]$ due to a gas of collapsed dipoles.

We start by rewriting the quantity $U(V,T)$ defined in (2.7) in terms of a diagrammatic expansion,

$$U(V,T) = \sum_{n=1}^{\infty} U_n . \quad (3.2)$$

The quantity U_n is the sum of all arrangements of $2n$ charges complying with the rules stated above. The procedure is then as follows. (1) We have to draw all possible bare diagrams with $2n$ charges of total charge zero which cannot be subdivided into disjoint neutral parts, and the first charge has to be $\xi_1 = -1$. (2) In the next step, the bare diagrams are dressed by decorating all odd time intervals τ_{2j-1} $(j = 1, \ldots, n)$ with square boxes. Each of the square boxes symbolizes insertion of a grand canonical gas of collapsed dipoles, i.e., a factor of $\exp[-\bar{\gamma}\tau_{2j-1}]$.

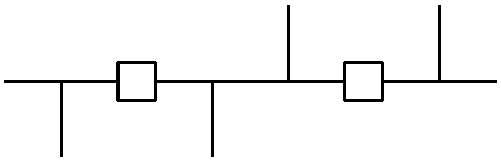


FIG. 3. Diagram giving the contribution U_2.

As outlined before, there are no such insertions for even time intervals τ_{2j}. To avoid double counting, integrations over even times are free of collapsed contributions, and therefore we restrict these integrations to $\bar{\gamma}\tau_{2j} > 1$. The term U_n contributes to order ϵ^{n-1} (and to higher orders). To illustrate this, the diagrams representing the terms U_1 to U_4 are shown in Figs. 2 to 5. While in orders $n = 1$ and $n = 2$ only one diagram is found, respectively, there are two diagrams for $n = 3$ and five diagrams for $n = 4$.

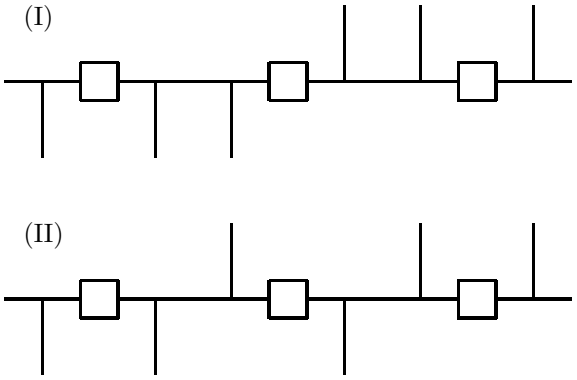


FIG. 4. The 2 diagrams yielding the contribution U_3.

The dressed diagram U_1 yields already the exact solution for $g = 1/2$ since all other contributions are at least of order ϵ. From Eq. (2.7), we find

$$U_1 = -V_0^2 \int_0^\infty d\tau \, \exp[-(\bar{\gamma} + ieV/2)\tau - S(\tau)] \, ,$$

which gives indeed the exact solution for $g = 1/2$ in terms of the digamma function $\psi(z)$,

$$G(V,T)/G_0 = 1 - \frac{2\gamma}{eV} \, \mathrm{Im}\, \psi \left(\frac{1}{2} + \frac{\gamma + ieV/2}{2\pi k_\mathrm{B} T} \right) \, . \quad (3.3)$$

Thus the notion of collapsed dipoles provides a remarkably simple derivation of this important result.[13] For finite ϵ, the quantity U_1 is the same as for $g = 1/2$ within leading-log accuracy, except for γ being replaced by $\bar{\gamma}$. At this point, we would like to remark that the diagram U_1 gives the correct limiting behavior $G/G_0 \to 0$ as $T \to 0$, $V \to 0$ for any V_0. Hence all higher-order dressed diagrams should give vanishing contributions in the zero-energy limit, and this indeed we find.

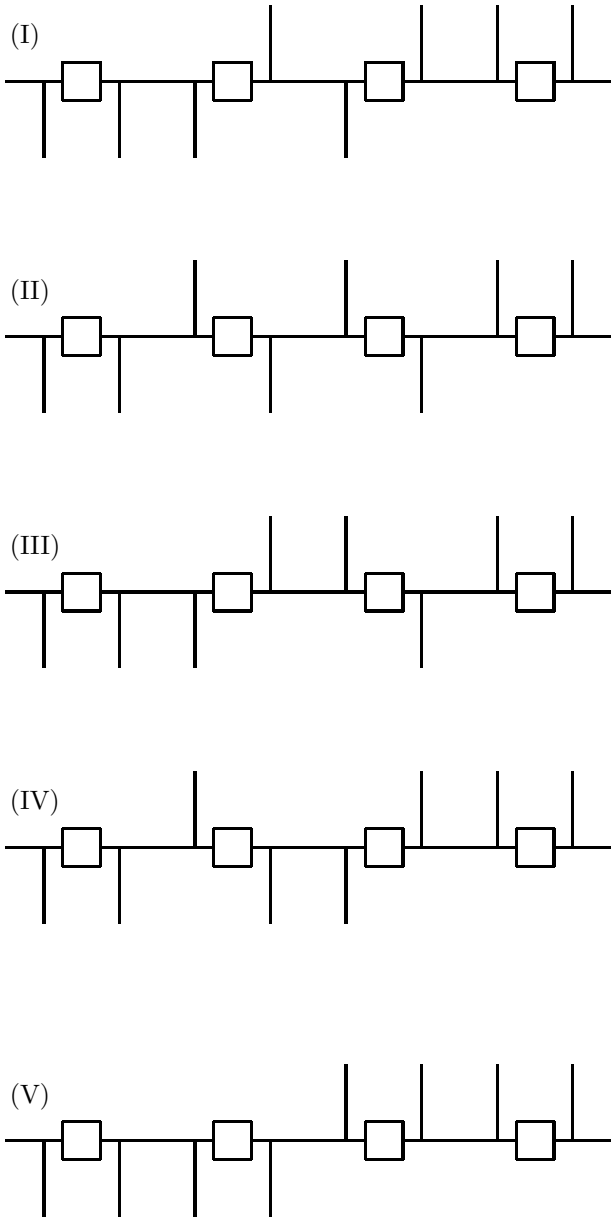


FIG. 5. The 5 diagrams contributing to U_4. Diagrams (I) – (IV) are of type (A), and diagram (V) is of type (B).

Generally, besides the lowest-order diagram in Fig. 1 we may distinguish two types of dressed diagrams. Diagrams of type (A) are of the form $(--X++)$. Here, X stands for insertion of any arrangement of *extended dipoles* $(+-)$ or $(-+)$ between the outer double charges $(--)$ and $(++)$.[19] Since there are two types of extended dipoles, we have 2^{n-2} dressed diagrams of type (A) contributing to order U_n. These dipoles are of finite length in contrast to the collapsed dipoles considered before. Hence they are interacting with each other and also with the outer charge pairs. However, because of the insertions of collapsed dipoles (indicated by the squares in the diagrams), they are narrow compared to typical inter-dipole

distances. All other diagrams contain at least four pairs of equal charge. We shall refer to them as diagrams of type (B). The simplest one of this type contributes to U_4 and is diagram (V) in Fig. 5. Remarkably, up to order U_3 only diagrams of type (A) are encountered.

Now we have to extract and evaluate the leading logarithmic contributions in the terms with $n > 1$. It simplifies notation to use scaled times and energies henceforth,

$$x_j = \bar{\gamma}\tau_j \ , \quad u = 2\pi k_{\rm B}T/\bar{\gamma} \ , \quad v = 2igeV/\bar{\gamma} \ . \tag{3.4}$$

According to the conditions (2.3), we are interested in the asymptotic regime

$$u \ll 1 \ ; \qquad |v| \ll 1 \ . \tag{3.5}$$

Now every *odd* time integration $\int dx_{2j+1}$ has a weight function $\exp(-x_{2j+1})$ due to the insertion of collapsed dipoles while all *even* time integrations are free of this weight. Hence it follows that the expression U_n is dominated by the regime

$$x_{2j+1} \ll x_{2k} \ , \qquad j,k = 0,1,\ldots,n-1 \ , \tag{3.6}$$

and the logarithms we wish to extract must arise from the integrations over the long even times. In the following, we describe in detail the general strategy we have employed to evaluate diagrams like the ones shown in Figs. 2–5.

We first rewrite the interaction factor (2.8) using the definitions

$$M_n = \exp \sum_{j>k=1}^{2n} \xi_j R(x_{jk}) \xi_k \ , \tag{3.7}$$

$$N_n = (2/u)^{2n\epsilon} M_n^{-2\epsilon} \ , \tag{3.8}$$

$$R(x) = \sinh(ux/2) \ , \tag{3.9}$$

such that

$$W_n = (\bar{\gamma}/\omega_{\rm c})^{(1-2\epsilon)n} \, (u/2)^n \, M_n N_n \ . \tag{3.10}$$

The factor M_n includes the interactions of $2n$ charges for $g = 1/2$, while the factor N_n encapsulates the remaining ϵ-dependent part of the interactions. The usefulness of the split-up (3.10) is demonstrated now.

Having drawn a certain diagram contributing to U_n, say $U_n^{(j)}$, we take advantage of a general decomposition theorem for the interaction factor M_n in (3.7). The decomposition theorem corresponds to Wick's theorem[20] for fermionic fields and originates from the equivalence of the interaction factor $\exp(-S(\tau))$ for $g = 1/2$ with a free 1D fermion propagator.[18] By virtue of this theorem, we can decompose M_n — which contains $n(2n-1)$ pair interactions — into a sum of $n!$ terms containing only n intrapair interactions of neutral pairs. This procedure results in the corresponding decomposition of a given nth order diagram into $n!$ graphs. The split-up (3.10) allows us therefore to *topologically reduce the diagrams to graphs which are much easier to evaluate*. Thereby the quantity U_n takes the form of a sum over all diagrams (labelled by an index (j)) where each diagram is represented by a sum of $n!$ graphs,

$$U_n = \frac{\epsilon^{n-1} u^n \bar{\gamma}}{2\pi} \ \sum_j \sum_{r=1}^{n!} U_n^{(j,r)} \ , \tag{3.11}$$

where $U_n^{(j,r)}$ describes the contribution of the rth graph to the nth-order diagram j under study (with the prefactor chosen accordingly). Pictorially, one obtains the graphs by grouping the $2n$ charges into n neutral pairs. Clearly, there are $n!$ different assignments and hence $n!$ different graphs for each diagram, with the sign of each graph given by the number of crossings of lines connecting the paired charges. Fig. 6 shows the 2 graphs for the diagram in Fig. 3 resulting in U_2, and in Fig. 7 the 12 graphs due to the two diagrams of U_3 are displayed.

In the final step, we group all graphs $U_n^{(j,r)}$ into *classes* with respect to their particular dependence on the even time intervals x_{2j}. Each of these classes is then evaluated in leading-log accuracy, and the remaining odd time integrations can be carried out without further approximation.

So far we have not taken into account the residual interaction factor N_n given in (3.8). We have to treat this term separately as it does not fit into the decomposition scheme. Under condition (3.6) and within leading-log accuracy, this factor has the same form for all diagrams of type (A) and is

$$N_n^{(A)} = (x_2 + x_4 + \cdots + x_{2n-2})^{8\epsilon} \ . \tag{3.12}$$

Unfortunately, for graphs of type (B), it is not so straightforward to include the factor N_n in the explicit calculation. Therefore, in this paper, we confine ourselves to the regime where it is consistent to put $N_n^{(B)} = 1$ (see Sec. IV C and Appendix).

IV. LEADING-LOG EVALUATION OF THE CONDUCTANCE

Following the general diagrammatic approach outlined in the previous section, we have explicitly calculated the leading logs in the expressions U_n for $n \le 4$. For larger n, the explicit calculation of all diagrams becomes prohibitively cumbersome. However, for the asymptotic low-energy corrections only the restricted set of diagrams of type (A) contributes, as we shall explain below. This permits an exact evaluation of the asymptotic corrections. The corresponding summation of all diagrams of type (A) is carried out in Sec. V A. In the remainder of this section, we illustrate the computation of U_n for $n \le 4$. That will also lead us towards the exact solution of this problem, see Sec. V B.

A. Contribution U_2

To proceed according to the strategy of Sec. III, we have to first draw all diagrams in order $n = 2$. There is only the single diagram shown in Fig. 3, which is of type (A) and contributes in order ϵ (and higher orders) to the series (3.1). In a second step, this diagram may be topologically reduced into the two graphs shown in Fig. 6, as follows from the decomposition of the interaction factor

$$M_2 = e^{R(x_1)+R(x_3)-R(x_2)-R(x_1+x_2)-R(x_2+x_3)-R(x_1+x_2+x_3)} = e^{-R(x_2)-R(x_1+x_2+x_3)} - e^{-R(x_1+x_2)-R(x_2+x_3)} ,$$

where $R(x)$ is given by Eq. (3.9). Both graphs fall into different classes, i.e. they have a different functional dependence on the long even time interval x_2. In particular, according to Eqs. (2.7) and (3.11), we have to evaluate the terms

$$U_2^{(1)} = \int_0^\infty dx_1 dx_3 \int_1^\infty dx_2 \times \frac{x_2^{8\epsilon}\, e^{-[1+v/2](x_1+x_3)-vx_2}}{\sinh[u(x_2+x_1+x_3)/2]\sinh[ux_2/2]} ,$$

$$U_2^{(2)} = -\int_0^\infty dx_1 dx_3 \int_1^\infty dx_2 \times \frac{x_2^{8\epsilon}\, e^{-[1+v/2](x_1+x_3)-vx_2}}{\sinh[u(x_2+x_1)/2]\sinh[u(x_2+x_3)/2]} ,$$

where we have used (3.12). Recalling that the dominant contributions to the triple integrals come from the region $x_1, x_3 \ll x_2$, it is clear that the logarithms which we wish to extract arise from the x_2-integrals. To proceed, we use the approximation

$$\frac{u\exp[ux+u(a+b)/2]}{4\sinh[u(x+a)/2]\sinh[u(x+b)/2]} \approx \frac{(1-e^{-u(b-a)})^{-1}}{x+a} + \frac{(1-e^{u(b-a)})^{-1}}{x+b} , \tag{4.1}$$

where x corresponds to the long even time x_2 and a, b are linear combinations of short odd times x_1, x_3. The terms neglected on the r.h.s. are subleading as they do not give logarithmic contributions. It is at this point where we invoke the leading-logarithmic approximation.

Identifying a and b with q, the contributions to the integral over the even time are in the form

$$\int_1^\infty dx \frac{x^{8\epsilon}}{x+q} e^{-(u+v)x} = e^{q(u+v)} L_2(\epsilon) . \tag{4.2}$$

Since the odd time integrations produce a purely imaginary contribution, we need to consider only the real part of $L_2(\epsilon)$, i.e. we may replace $u+v$ by $|u+v|$ in this term when performing these integrations. Within leading-log accuracy, we have

$$L_2(\epsilon) = \int_1^\infty dx \frac{e^{-|u+v|x}}{x^{1-8\epsilon}} = -\ln|u+v| \Big(1 + O(\epsilon \ln|u+v|)\Big) . \tag{4.3}$$

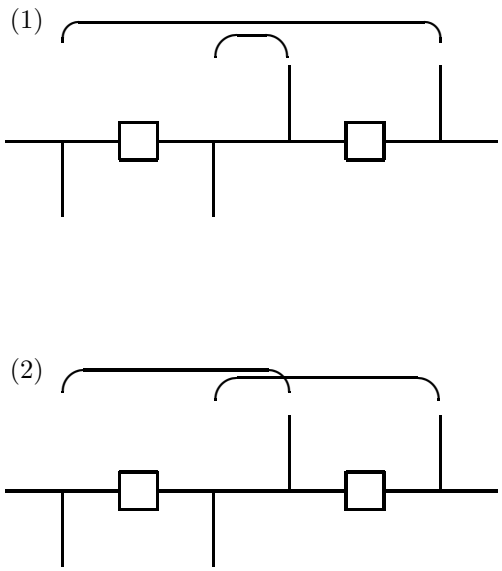


FIG. 6. The two graphs obtained from the decomposition theorem for the contribution U_2 shown in Fig. 3. The relative signs are + for graph (1) and − for graph (2). The curves display interactions between paired charges.

Upon using Eqs. (4.1) and (4.2), the resulting expressions for $U_2^{(1)}$ and $U_2^{(2)}$ may be combined in a form which will find straightforward generalization to higher orders,

$$\mathrm{Im}\sum_r U_2^{(r)} = -\frac{2}{u} L_2(\epsilon) \int_0^\infty dx_1 dx_3\, e^{-(x_1+x_3)} \times \sum_{\{\sigma_j=\pm 1\}} \sigma_1\sigma_3 \frac{\sin[|v|(\sigma_1 x_1+\sigma_3 x_3)/2]}{\sinh[u(\sigma_1 x_1+\sigma_3 x_3)/2]} . \tag{4.4}$$

The remaining odd time integrations pose no problem and are done easily.

Collecting all terms together, we find the leading-log contributions to the conductance resulting from U_2 in all orders in ϵ,

$$\mathrm{Im}\, U_2 = 4\epsilon \frac{\bar\gamma}{\pi} L_2(\epsilon)\, \mathrm{Im}\Big[\psi\left(\frac{2+u+v}{2u}\right) + u^{-1}\psi'\left(\frac{2+u+v}{2u}\right)\Big] . \tag{4.5}$$

The function ψ' is the derivative of the ψ function. Together with the contribution due to U_1, this gives *all* terms in order ϵ (plus partial summation of higher-order terms in ϵ).

B. Contribution U_3

To proceed further, let us now study the next order. The two diagrams contributing to order U_3 are displayed

in Fig. 4. Applying the before-mentioned decomposition scheme for the interaction factor M_3, we find the 12 graphs shown in Fig. 7. Again we group them into classes regarding their dependence on the even intervals x_2, x_4. The contributions $U_3^{(j,r)}$ $(j = 1, 2;\, r = 1, \ldots, 6)$ corresponding to the 12 graphs in Fig. 7 are expressed as

$$U_3^{(1,\,r=1,\ldots,6)} = \int_0^\infty dx_1 dx_3 dx_5 \int_1^\infty dx_2 dx_4 \times e^{-[1+v/2](x_1+x_3+x_5)-vx_3}\, e^{-v(x_2+x_4)}\, N_3^{(A)} f_3^{(1,r)}$$

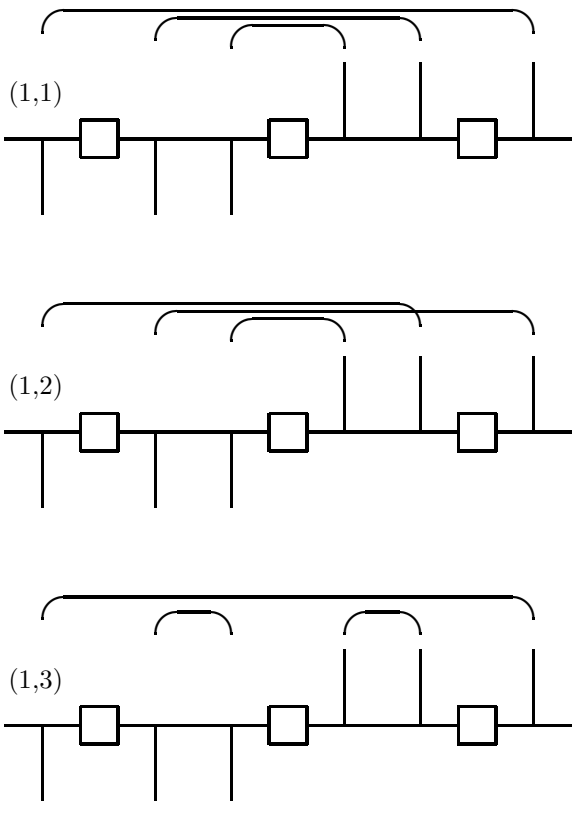
$$U_3^{(2,\,r=1,\ldots,6)} = \int_0^\infty dx_1 dx_3 dx_5 \int_1^\infty dx_2 dx_4 \times e^{-[1+v/2](x_1+x_3+x_5)}\, e^{-v(x_2+x_4)}\, N_3^{(A)} f_3^{(2,r)}\,,$$

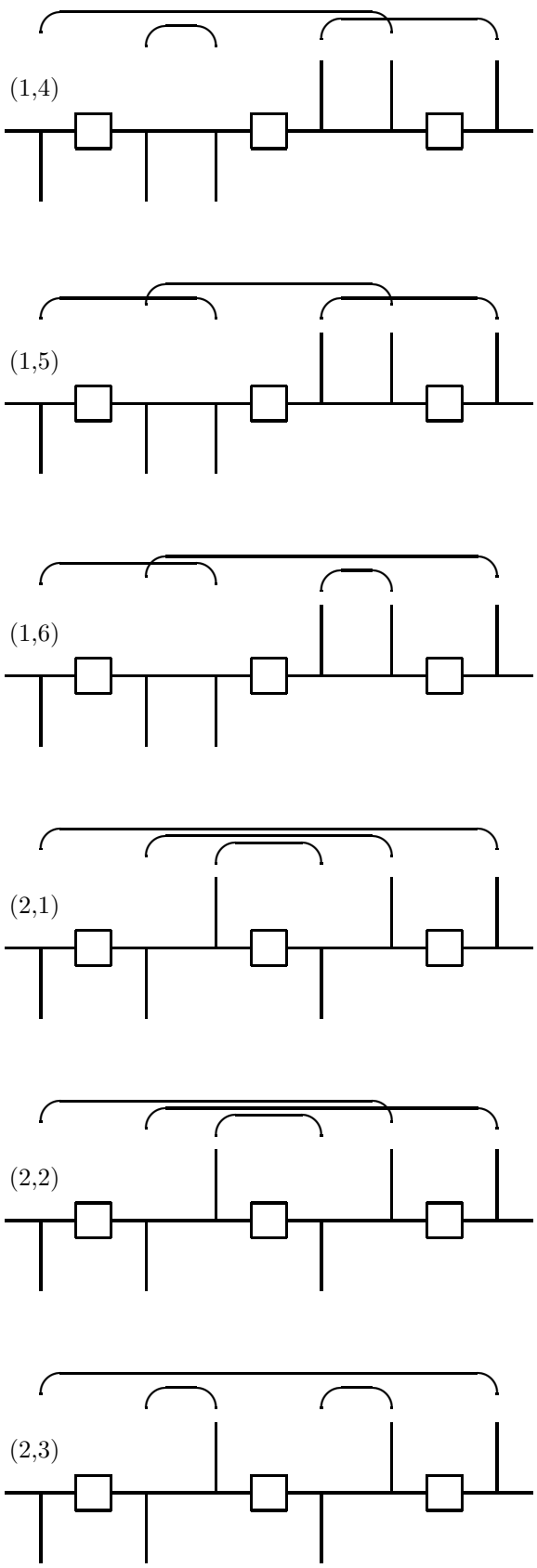
where $N_n^{(A)}$ is given in (3.12), and where each $f_3^{(j,r)}$ belongs to one of the following two classes,

$$f_3^{(1)} = \Big(\sinh[u(x_2+x_4+a)/2] \times \sinh[u(x_2+x_4+b)/2]\sinh[uc/2]\Big)^{-1}\,,$$

$$f_3^{(2)} = \Big(\sinh[u(x_2+a)/2] \times \sinh[u(x_4+b)/2]\sinh[u(x_2+x_4+c)/2]\Big)^{-1}\,.$$

Here, a, b, c denote certain linear combinations of the short odd time intervals $x_1, x_3, x_5 \ll x_2, x_4$. This classification is again motivated by the fact that logarithmic terms are attributed to the domain of long even time intervals.





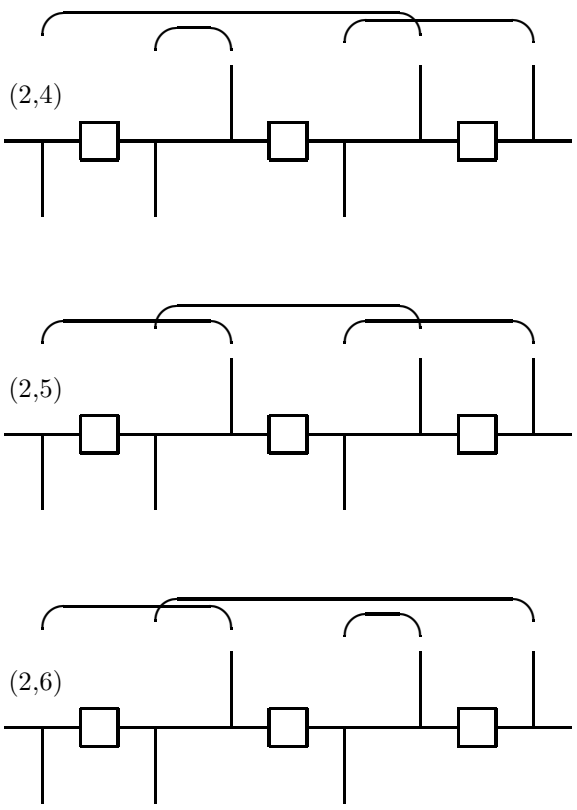


FIG. 7. The 12 graphs obtained from the 2 diagrams in order U_3 shown in Fig. 4. The graphs $(1,1),(1,3),(1,5),(2,1),(2,3)$, and $(2,5)$ have positive sign, the remaining ones are negative.

From Fig. 7 it is obvious that the graphs (1,1),(1,2),(2,1), and (2,2) fall into the class $f_3^{(1)}$, whereas all other graphs belong to the class $f_3^{(2)}$. To identify the classes giving leading logs, we put $N_A^{(3)}=1$ for the moment. Then, in performing the even time integrations, we have to look for terms giving squares of logarithms, $\ln^2|u+v|$. Upon using Eq. (4.1), it is easily shown that the first class $f_3^{(1)}$ gives subleading terms $\sim\ln|u+v|$ only, and solely the eight diagrams in the second class produce leading logs. The even time integrations are tackled by switching to the variables

$$x=x_2+x_4\ ,\quad \rho=(x_2-x_4)/2\ ,$$

which allows for exact evaluation of the ρ integral. As the logarithms come from the region $x_1,x_3,x_5\ll x$, the x-integral takes the same form for the eight remaining graphs. Upon performing a substitution $x+q\to x$ as given in (4.2) with (4.3), where now q is a, b or c, the logarithms of $|u+v|$ are in the integral

$$\begin{aligned} L_3(\epsilon) &= \int_1^\infty dx\,\frac{\ln x}{x^{1-8\epsilon}}\,e^{-|u+v|x} \qquad (4.6)\\ &= \frac{1}{2}\ln^2|u+v|\,\Big(1+O(\epsilon\ln|u+v|)\Big)\ , \end{aligned}$$

where we have reintroduced $N_A^{(3)}=x^{8\epsilon}$. Labelling the relevant 8 graphs with variables $\sigma_1,\sigma_3,\sigma_5=\pm1$, the imaginary part of the sum of them can be written in the compact form

$$\begin{aligned} \mathrm{Im}\sum_{j,r}U_3^{(j,r)} &= \frac{16}{u^2}L_3(\epsilon)\int_0^\infty dx_1dx_3dx_5\,e^{-(x_1+x_3+x_5)}\\ \times\sum_{\{\sigma_j=\pm1\}}\sigma_1\sigma_5\,&\frac{\sin[|v|(\sigma_1x_1+\sigma_3x_3+\sigma_5x_5)/2]}{\sinh[u(\sigma_1x_1+\sigma_3x_3+\sigma_5x_5)/2]}\ . \qquad (4.7) \end{aligned}$$

Here, the factor $\sigma_1\sigma_5$ gives the signs of the respective graphs.

To evaluate the remaining odd time integrations, it is useful to insert the identity in form of

$$1=\int_{-\infty}^\infty ds\int_{-\infty}^\infty\frac{dk}{2\pi}\,e^{ik[s-(\sigma_1x_1+\sigma_3x_3+\sigma_5x_5)]}\ . \qquad (4.8)$$

Performing the summation over the σ's and the integration over x_1,x_3,x_5, one finds a factor $-8k^2/[1+k^2]^3$, and we are left with the k- and s-integrals. These can be carried out analytically, and we obtain the leading-log terms of U_3 in the form

$$\begin{aligned} \mathrm{Im}\,U_3 &= -4\epsilon^2\,\frac{\bar\gamma}{\pi}\,L_3(\epsilon)\,\mathrm{Im}\Big[\psi\left(\frac{2+u+v}{2u}\right) \qquad (4.9)\\ &\quad --u^{-1}\psi'\left(\frac{2+u+v}{2u}\right)-u^{-2}\psi''\left(\frac{2+u+v}{2u}\right)\Big]\ . \end{aligned}$$

This gives together with U_1 and U_2 all leading-log contributions to the mobility up to order ϵ^2.

C. Contribution U_4

To understand the general structure of all higher-order terms, it is very illuminating to study the next contribution. Although this is quite tedious, it will turn out to guide us towards an exact summation of *all* diagrams relevant for the asymptotic low-energy behavior. The five diagrams contributing to U_4 are shown in Fig. 5. Each of them can be decomposed into $4!=24$ graphs, yielding 120 graphs in total. Diagrams (I) to (IV) are of type (A), while diagram (V) is of type (B). Since the calculation of U_4 is somewhat lengthy but proceeds along the same lines as in Secs. IV A and IV B, the relevant technical details are given in the Appendix. In this section, we only discuss some conclusions obtained from this computation.

The main findings are exhibited in Eqs. (A3) and (A4) of the Appendix which show that there is a crucial difference between diagrams of type (A) and type (B). In type-(A) diagrams, one has a product of only two σ's in the integrand, while diagrams of type (B) contain at least four σ factors. This characteristic behavior directs us towards an important conclusion. Upon pulling out a factor $L_4(0)|v|/u^4$ in Eq. (A4), we may expand the remaining expression in powers of u^2 and $|v|^2$. Now, because of the

σ-factors, terms up to order u^2 and $|v|^2$ cancel out in the sum over $\{\sigma\}$, and nonvanishing contributions from the odd time integrations are at least of order $u^4, |v|^4, u^2|v|^2$. Since the asymptotic low-energy behavior in Eq. (3.1) is governed by $a_j \sim u^2, |v|^2$, it is obvious that the asymptotic properties are entirely unaffected by diagram (V). It is immediately clear that also all higher-order diagrams of type (B) do not contribute to coefficients $a_j \sim u^2, |v|^2$. From this we conclude that, while the zero-energy value of the conductance $G = 0$ is fully determined by the diagram shown in Fig. 2, *the asymptotic corrections in u and $|v|$ are completely governed by diagrams of type (A)*. Following this observation, one can make further progress. This will be discussed in Section V A.

Let us finally collect together all contributions in order ϵ^3 due to $\mathrm{Im}\, U_4$ for arbitrary powers in u^2 and $|v|^2$. Using again an identity of the form (4.8), the integrals (A3) and (A4) given in the Appendix can be evaluated exactly. In the end, we find

$$\mathrm{Im}\, U_4 = 64\epsilon^3 \frac{\bar\gamma}{\pi} L_4(0)\, \mathrm{Im}\left[\psi\left(\frac{2+u+v}{2u}\right)\right. \tag{4.10}$$
$$- u^{-1}\psi'\left(\frac{2+u+v}{2u}\right) + 2u^{-2}\psi''\left(\frac{2+u+v}{2u}\right)$$
$$\left. + u^{-3}\psi^{(3)}\left(\frac{2+u+v}{2u}\right)\right].$$

In view of the increasing complexity it appears to be prohibitive to go beyond order ϵ^3 in all powers of $u^2, |v|^2$. However, as the expansion is already well advanced, in the next section the findings obtained so far will be taken up to conclude on exact results.

V. RESULTS

A. Asymptotic low-energy corrections

Our analysis in the previous section suggests that one can sum the whole leading-log series (3.1) for the contributions $a_j \sim u^2, |v|^2$, where scaled temperature u and bias v are given in Eq. (3.4). These contributions determine the asymptotic low-energy properties of the transport process. The leading-log summation can indeed be performed in all orders by considering only the asymptotic regime. As shown in the previous section, the only diagrams contributing to this regime are of type (A). The sum of all of them can be expressed as $(--Y++)$, where Y stands for the grand canonical gas of finite-length dipoles of the two types $(+-)$ and $(-+)$. (So Y is basically a sum over all arrangements X mentioned in Sec. III.) In the remainder of this subsection, we will ignore all other diagrams.[22]

The contribution $U_n^{(A)}$ to U_n due to diagrams of type (A) can now be evaluated *in every order n*. The even time integrals result in a function $L_n(\epsilon)$ containing the logarithm,

$$L_n(\epsilon) = \frac{1}{(n-2)!}\int_1^\infty dx\, \frac{\ln^{n-2} x}{x^{1-8\epsilon}}\, e^{-|u+v|x}\,. \tag{5.1}$$

Here, we have already integrated out all even time intervals except the totally symmetric combination $x = x_2 + \ldots + x_{2n-2}$, and we have included the interaction factor (3.12). Taking into account the remaining odd time integrals and summing over all possible arrangements of the intermediate dipoles, we find

$$\mathrm{Im}\sum_{j\in(A),\,r} U_n^{(j,r)} = (-1)^{n-1}\frac{8^{n-1}}{4u^{n-1}} L_n(\epsilon) \tag{5.2}$$
$$\times \int_0^\infty dx_1\cdots dx_{2n-1}\, e^{-(x_1+\cdots+x_{2n-1})}$$
$$\times \sum_{\{\sigma_j=\pm1\}} \sigma_1\sigma_{2n-1}\, \frac{\sin[|v|(\sigma_1 x_1+\cdots+\sigma_{2n-1}x_{2n-1})/2]}{\sinh[u(\sigma_1 x_1+\cdots+\sigma_{2n-1}x_{2n-1})/2]}\,.$$

Upon expanding the integrand, we find to lowest order in u and $|v|$ the nth contribution to the conductance ($n > 1$)

$$\frac{G^{(n)}}{G_0} = -2\epsilon\frac{|u+v|^2}{12}\frac{(-16\epsilon)^{n-2}}{(n-2)!}\int_1^\infty dx\, \frac{\ln^{n-2} x}{x^{1-8\epsilon}}\, e^{-|u+v|x}\,.$$

Finally, summing over all n gives to lowest integer orders in u and $|v|$ the expression

$$\frac{G}{G_0} = \frac{1}{12}|u+v|^2\left(1 - 8\epsilon\int_1^\infty dx \frac{e^{-|u+v|x}}{x^{1+8\epsilon}}\right)\,. \tag{5.3}$$

An important feature should be noted. If one stops the expansion at the term $n = 2$, an expression of the form (5.3) would emerge with the factor $x^{8\epsilon}$ in the denominator of the integrand replaced by $x^{-8\epsilon}$. The whole nonperturbative effect of inserting a grand canonical gas of finite-length dipoles between the charge pairs $(--)$ and $(++)$ simply results in exchanging the factor $x^{-8\epsilon}$ in the denominator of the integrand for the factor $x^{8\epsilon}$, as it is already done in the integrand of (5.3). Clearly, this substitution leads to a crucial change in the dependence on u and $|v|$.

Upon performing the integral, we finally get the *exact asymptotic behavior*

$$G(V,T)/G_0 = (1/3)\left[(eV/2k_{\mathrm{B}}T_{\mathrm{K}})^2 + (\pi T/T_{\mathrm{K}})^2\right]^{1+4\epsilon}\,. \tag{5.4}$$

This result is valid under conditions (2.3). For the linear conductance, the $T^{2/g-2}$ behavior found by KF is indeed recovered. More generally, the low-temperature corrections to the zero-temperature nonlinear conductance will follow this law as long as $eV \ll k_{\mathrm{B}}T$. However, if $eV \gg k_{\mathrm{B}}T$, one finds a g-independent universal T^2 law. Clearly, for any finite value of the external voltage, the

ultimate low-temperature behavior should then be T^2. The result (5.4) describes a smooth turnover between these two power laws and demonstrates unambiguously that the limits $V \to 0$ and $T \to 0$ do not commute.

The nonanalytical form of the conductance is due to the critical nature of the ($T = V = 0$) model. Inclusion of a finite voltage breaks scale invariance, and if one considers the temperature dependence under $V \neq 0$, analytical behavior will be observed. The physical reason for T^2 corrections is the low-frequency thermal noise of the plasmon modes in the leads.[23] Similar low-temperature T^2 features can be found in a number of different systems where Ohmic damping is present.[13] We believe that these universal T^2 features can indeed be observed in the $g = \nu = 1/3$ FQH transport experiments of Milliken *et al.*[4] Experiments have so far been carried out at small source-drain voltage $eV/k_{\rm B}T \approx 0.2$, and hence the KF T^4 law has been found. It would be interesting to explore the regime $eV \gg k_{\rm B}T$, where one should be able to see the T^2 law. Sample heating is not expected to cause major problems since G is still quite small. Finally we mention a completely different experimental possibility for detection of this crossover from $T^{2/g-2}$ to T^2 behaviors, namely the novel quantum wire experiments by Tarucha *et al.*[6]

B. Conjectured exact result

Our explicit calculation for U_n up to order $n = 4$ in Sec. IV as well as the exact summation of the leading-log series (3.1) to lowest order $u^2, |v|^2$ allow us to conjecture on the asymptotically exact result. All these results are consistent with the following expression for the mobility

$$\frac{G(V,T)}{G_0} = 1 - \frac{2\gamma_{\rm r}}{eV}\,{\rm Im}\,\psi\left(\frac{1}{2} + \frac{\gamma_{\rm r} + ieV/2}{2\pi k_{\rm B}T}\right)\ , \qquad (5.5)$$

which is just the exact solution (3.3) for $g = 1/2$ with a *voltage- and temperature-dependent renormalization*

$$\gamma \to \gamma_{\rm r} = \bar\gamma\left((eV/2\bar\gamma)^2 + (\pi k_{\rm B}T/\bar\gamma)^2\right)^{-2\epsilon}\ . \qquad (5.6)$$

We remind the reader that $\bar\gamma/k_{\rm B}$ is just the Kondo temperature. Expanding Eq. (5.5) in powers of ϵ, one finds exactly all contributions up to order ϵ^3 — but in all orders of $u^2, |v|^2$ — as derived in Sec. IV. Similarly, when expanding Eq. (5.5) up to order $u^2, |v|^2$, we recover Eq. (5.4) in all orders of ϵ. Furthermore, the $T = 0$ limit of (5.5) coincides with very recent calculations by Fendley *et al.*[24]

It is tempting, in the light of these findings, to assert that the result (5.5) is the *exact* solution under conditions (2.3). This statement also receives support from the correspondence of our model with an interacting fermion model.[11] To make the correspondence, we rewrite the solution (5.5) in terms of a suitable momentum integral representation. Upon using the representation (x and y real)

$${\rm Im}\,\psi(1/2 + x + iy) = \int_0^\infty \frac{ds}{1+s^2}\Big(\frac{1}{e^{2\pi(xs-y)}+1} - \frac{1}{e^{2\pi(xs+y)}+1}\Big)$$

and putting $s = (v_{\rm F}p/\bar\gamma)^{1+4\epsilon}$, Eq. (5.5) takes the form

$$\frac{G}{G_0} = 1 - \frac{2v_{\rm F}}{eV}\int_0^\infty dp\, n(p)\,|S_{+-}(p)|^2 \times \Big(f[E(p) - eV/2] - f[E(p) + eV/2]\Big)\ , \qquad (5.7)$$

where $f(E)$ is the Fermi function, and where

$$|S_{+-}(p)|^2 = \left(1 + \left(\frac{v_{\rm F}p}{\bar\gamma}\right)^{2+8\epsilon}\right)^{-1}\ , \qquad (5.8)$$

$$n(p) = \left(\frac{(v_{\rm F}p)^2}{(eV/2)^2 + (\pi k_{\rm B}T)^2}\right)^{2\epsilon}\ . \qquad (5.9)$$

$$E(p) = v_{\rm F}p\, n(p) \qquad (5.10)$$

In the work by Fendley *et al.*,[11] a similar formula is derived for $g = 1/3$ using the thermodynamic Bethe ansatz and a Boltzmann rate expression. The function $|S_{+-}(p)|^2$ in (5.8) agrees with the form of the squared modulus of the exact S matrix of the quasiparticles for impurity scattering[15] on putting $g = 1/2 - \epsilon$. The function $n(p)$ represents the density of states of these quasiparticles at voltage V and temperature T in the regime (2.3). Finally, the quantity $E(p)$ is a pseudoenergy used to parametrize the occupation probability of the quasiparticles as $f[E(p)]$.

In conclusion, the results of our dynamical method are in full agreement with what one would expect from combining the thermodynamic Bethe ansatz with a Boltzmann rate expression. Moreover, we obtained the density of states and the pseudoenergy of the quasiparticles in explicit form for $g = 1/2 - \epsilon$.

VI. CONCLUDING REMARKS

We have studied transport properties of a Luttinger liquid through a barrier at low temperature and for small voltage. This nonperturbative problem has been approached by a leading-log summation technique which is valid near the value $g = 1/2$ of the interaction constant. Putting $g = 1/2 - \epsilon$, the leading logs have been summed up in all orders ϵ^n for the asymptotic low-energy regime. Furthermore, the conductance has been evaluated up to order ϵ^3 for all powers of V^2, T^2. Both findings allow to conclude on the exact result for the low-temperature conductance near $g = 1/2$. The asymptotic low-temperature corrections exhibit a smooth turnover from the $T^{2/g-2}$ law to a universal T^2 behavior as the voltage is increased. In fact, for any finite voltage, one should find the T^2 law for $k_{\rm B}T \ll eV$. We have also provided a simple

physical argument to explain the T^2 enhancement at finite voltage. These T^2 corrections can be found even in the presence of electron-electron backscattering. All these Luttinger liquid fingerprints should be observable with the fractional quantum Hall devices of Milliken *et al.*[4] We predict that application of a source-drain voltage drop $eV \gg k_{\rm B}T$ will change the KF T^4 law into a T^2 behavior.

To conclude, we mention that our method provides the unique possibility of performing exact noise calculations. It seems very difficult or even impossible to obtain ac noise properties with any other technique available at the moment.

ACKNOWLEDGMENTS

This work was partially supported by the EC SCIENCE program. We have benefitted from discussions with P. Fendley, L.I. Glazman, H. Grabert, F. Guinea, C.H. Mak, H. Saleur and A.D. Zaikin.

[1] J.M. Luttinger, J. Math. Phys. **4**, 1154 (1963); A. Luther and I. Peschel, Phys. Rev. B **9**, 2911 (1975); V.J. Emery, in *Highly conducting one-dimensional solids*, edited by J.T. Devreese *et al.* (Plenum, NY, 1979).
[2] F.D.M. Haldane, J. Phys. C **14**, 2585 (1981); Phys. Rev. Lett. **47**, 1840 (1981).
[3] X.G. Wen, Phys. Rev. Lett. **64**, 2206 (1990); Phys. Rev. B **44**, 5708 (1991); Int. J. Mod. Phys. B **6**, 1711 (1992).
[4] F.P. Milliken, C.P. Umbach and R.A. Webb, unpublished.
[5] G. Timp, in *Mesoscopic phenomena in solids*, ed. by B.L. Altshuler *et al.* (Elsevier, Amsterdam, 1990).
[6] S. Tarucha, T. Honda and T. Saku, Sol. Stat. Comm. **94**, 413 (1995).
[7] C.L. Kane and M.P.A. Fisher, Phys. Rev. Lett. **68**, 1220 (1992); Phys. Rev. B **46**, 15233 (1992).
[8] J. Solyom, Adv. Phys. **28**, 201 (1979).
[9] K.A. Matveev, D. Yue and L.I. Glazman, Phys. Rev. Lett. **71**, 3351 (1993); D. Yue, L.I. Glazman and K.A. Matveev, Phys. Rev. B **49**, 1966 (1994).
[10] K.A. Matveev and L.I. Glazman, Phys. Rev. Lett. **70**, 990 (1993).
[11] P. Fendley, A.W.W. Ludwig and H. Saleur, Phys. Rev. Lett. **74**, 3005 (1995).
[12] K. Moon, H. Yi, C.L. Kane, S.M. Girvin and M.P.A. Fisher, Phys. Rev. Lett. **71**, 4381 (1993).
[13] U. Weiss and M. Wollensak, Phys. Rev. B **37**, 2729 (1988); U. Weiss, M. Sassetti, T. Negele and M. Wollensak, Z. Phys. B **84**, 471 (1991).
[14] F. Guinea, Phys. Rev. B **32**, 7518 (1985).
[15] S. Ghoshal and A. B. Zamolodchikov, Int. J. Mod. Phys. A **9**, 3841 (1994).
[16] A. Schmid, Phys. Rev. Lett. **51**, 1506 (1983); M.P.A. Fisher and W. Zwerger, Phys. Rev. B **32**, 6190 (1985).
[17] R.P. Feynman and F.L. Vernon, Ann. Phys. (NY) **24**, 118 (1963).
[18] A. J. Leggett, S. Chakravarty, A. T. Dorsey, M. P. A. Fisher, A. Garg and W. Zwerger, Rev. Mod. Phys. **59**, 1 (1987).
[19] Note that their contributions cancel each other when they are collapsed as these dipoles are inserted into even time intervals.
[20] A.L. Fetter and J.D. Walecka, *Quantum Theory of Many-Particle Systems*, (McGraw-Hill, New York, 1971).
[21] I.S. Gradsteyn and I.M. Ryzhik, *Table of Integrals, Series and Products* (Academic Press, Inc., 1980).
[22] A systematic computation of the next-leading contributions $a_j \sim u^4, |v|^4, u^2|v|^2$ could be feasible by noticing that these are completely determined by diagrams of type $(--Y--+Y++)$ in addition to $(--Y++)$.
[23] J.M. Martinis and H. Grabert, Phys. Rev. B **38**, 2371 (1988); M. Sassetti and U. Weiss, Phys. Rev. Lett. **65**, 2262 (1990).
[24] P. Fendley, A.W.W. Ludwig and H. Saleur, preprint.

APPENDIX: CONTRIBUTIONS TO U_4

This appendix contains the technical details of the computation of the contribution U_4 to the conductance discussed in Sec. IV C. The 96 graphs related to the diagrams (I) to (IV) shown in Fig. 5 fall into four classes regarding their dependence on the long even times x_2, x_4, x_6. Denoting combinations of the short odd times as a, b, c, d, these four classes are given by

$$f_4^{(1)} = \Big(\sinh[u(x_2+a)/2]\sinh[u(x_4+b)/2] \times \sinh[u(x_6+c)/2]\sinh[u(x_2+x_4+x_6+d)/2]\Big)^{-1}$$

$$f_4^{(2)} = \Big(\sinh[u(x_2+a)/2]\sinh[u(x_6+b)/2] \times \sinh[u(x_2+x_4+c)/2]\sinh[u(x_4+x_6+d)/2]\Big)^{-1}$$

$$f_4^{(3)} = \Big(\sinh[u(x_4+a)/2]\sinh[u(x_4+b)/2] \times \sinh[u(x_2+x_4+x_6+c)/2] \times \sinh[u(x_2+x_4+x_6+d)/2]\Big)^{-1}$$

$$f_4^{(4)} = \Big(\sinh[u(x_4+a)/2]\sinh[u(x_2+x_4+b)/2] \times \sinh[u(x_4+x_6+c)/2]\sinh[u(x_2+x_4+x_6+d)/2]\Big)^{-1} .$$

Putting $N_4^{(A)} = 1$ for the moment in analogy to Sec. IV B, the triple integral

$$\int_1^\infty dx_2 dx_4 dx_6\, e^{-v(x_2+x_4+x_6)}\, f_4^{(r)} \qquad \text{(A1)}$$

must give the logarithms, and we are interested in terms $\sim \ln^3|u+v|$. It is straightforward to show that the class $f_4^{(3)}$ does not give leading logs. The other three classes, however, give leading logarithmic contributions.

Switching to relative times and to the variable $x = x_2 + x_4 + x_6$, the former are easily integrated out. Upon performing the shift $x+q \to x$, where q is a, b, c, or d, and restoring $N_4^{(A)} = x^{8\epsilon}$, the remaining integral resulting from Eq. (A1) is

$$L_4(\epsilon) = \frac{1}{2!}\int_1^\infty dx\, \frac{\ln^2 x}{x^{1-8\epsilon}}\, e^{-|u+v|x}\,. \tag{A2}$$

Having evaluated the even time integrals in this way, the remaining odd time integrals of the relevant graphs take forms such that the sum of them indeed gives an expression fitting to the previous forms (4.4) and (4.7),

$$\begin{aligned}\mathrm{Im}\sum_{j\in(A),\,r} U_4^{(j,r)} &= -\frac{128}{u^3}L_4(\epsilon)\int_0^\infty dx_1dx_3dx_5dx_7 \\ &\times e^{-(x_1+x_3+x_5+x_7)}\sum_{\{\sigma=\pm1\}}\sigma_1\sigma_7 \\ &\times \frac{\sin[|v|(\sigma_1x_1+\sigma_3x_3+\sigma_5x_5+\sigma_7x_7)/2]}{\sinh[u(\sigma_1x_1+\sigma_3x_3+\sigma_5x_5+\sigma_7x_7)/2]}\,.\end{aligned} \tag{A3}$$

This contains all contributions of graphs due to the type-(A) diagrams (I) to (IV). Using the same procedure as before for U_3, this expression can be evaluated without any further approximation. Before stating the result, we discuss the remaining diagram (V) in Fig. 5.

The 24 graphs related to diagram (V) fall into three classes. One is just $f_4^{(3)}$ from above and does not contribute to leading logarithms. Another one is $f_4^{(4)}$ and does contribute. The third and last type is of the form

$$\begin{aligned}&\Big(\sinh[u(x_2+x_4+a)/2]\sinh[u(x_2+x_4+b)/2] \\ &\times\sinh[u(x_4+x_6+c)/2]\sinh[u(x_4+x_6+d)/2]\Big)^{-1}\end{aligned}$$

and does not contribute to leading logs. In view of the before-mentioned complications of the even time integrations due to the residual interaction factor $N_4^{(B)}$, we restrict our attention to the order ϵ^3 in the diagram (V), i.e. we put $N_4^{(B)} = 1$ and do not push the explicit calculation beyond this order. Carrying out the even time integrations as before, we then find the factor $L_4(0)$.

The remaining odd time integrals of the relevant graphs can be written in such a form that the contribution of diagram (V) emerges as

$$\begin{aligned}\mathrm{Im}\sum_{j\in(B),\,r} U_4^{(j,r)} &= \frac{64}{u^3}L_4(0)\int_0^\infty dx_1dx_3dx_5dx_7 \\ &\times e^{-(x_1+x_3+x_5+x_7)}\sum_{\{\sigma_j=\pm1\}}\sigma_1\sigma_3\sigma_5\sigma_7 \\ &\times \frac{\sin[|v|(\sigma_1x_1+\sigma_3x_3+\sigma_5x_5+\sigma_7x_7)/2]}{\sinh[u(\sigma_1x_1+\sigma_3x_3+\sigma_5x_5+\sigma_7x_7)/2]}\,.\end{aligned} \tag{A4}$$

The crucial difference to the expression (A3) for diagrams (I) to (IV) is the sign factor $\sigma_1\sigma_3\sigma_5\sigma_7$ instead of $\sigma_1\sigma_7$. These distinguishing features are easily extended to higher-order diagrams $n > 4$ as follows. Every *odd* time interval τ_{2j-1} that is fenced by charges of the same sign gives a factor σ_{2j-1} in the integrands of the respective functions $\mathrm{Im}\sum_{j\in(A),\,r} U_n^{(j,r)}$ and $\mathrm{Im}\sum_{j\in(B),\,r} U_n^{(j,r)}$, see Eqs. (A3) and (A4). Diagrams of type (A) involve a product of only two $\sigma's$ in the integrand, while diagrams of type (B) imply a product of at least four $\sigma's$. The final result for U_4 and the consequences of this observation are discussed in detail in Sec. IV C.